Wetting and Active Dewetting Processes of Hierarchically Constructed Superhydrophobic Surfaces Fully Immersed in Water

Choongyeop Lee and Chang-Jin "CJ" Kim, *Member, IEEE*

***Abstract*—When a superhydrophobic (SHPo) surface is fully submerged underwater, the surface becomes wet eventually and cannot recover the SHPo state naturally. In this paper, we fabricate hydrophobic microposts on a hydrophobic nanostructured substrate, i.e., hierarchically structured SHPo surfaces, and investigate their wetting and dewetting processes while immersed in water. All the micropost surfaces get wet, with the conditions of the water only affecting the speed of wetting. All the nanopost surfaces get wet over time after all the microposts on them are wetted. We demonstrate various active means (saturating air in water, bridging the surface to the outside air, and gas generation on the substrate) that can dewet the already wetted microposts as far as the substrate nanoposts remained nonwet. In particular, the SHPo surfaces with the recently developed electrolytic recovery mechanism are shown to maintain an SHPo state even under previously irreconcilable conditions, such as surface defects and high liquid pressure, indefinitely. [2011-0221]**

***Index Terms*—Dewetting, hierarchical surface, superhydrophobic (SHPo), surface engineering, surface texture.**

I. Introduction

A. SHPo Surfaces

INSPIRED by the unique properties of lotus leaves [1] and encouraged by the possibility of engineering similar surfaces with microfabrication techniques [2], superhydrophobic (SHPo) surfaces have been the object of intensive research interests in various disciplines spanning chemistry, materials science, and engineering [3]–[6]. Most of the early studies were to understand how a water droplet interacts with SHPo surfaces [7] and to fabricate them with different functionalities, e.g., a large sample area [8], optical transparency [9], or mechanical robustness [10]. In addition to the scientific interests with droplets, the recent studies have shown that the SHPo surfaces can also be useful for underwater applications (i.e., involving a continuous flow) by reducing frictional drag [11]–[18], promoting interfacial transport phenomena [19], and suppressing biofouling [20], [21]. For instance, a giant liquid slip—large enough to affect even regular-scale fluidic systems—was obtained on optimally designed microstructures [14]–[16], and drag reduction by the surface slip was reported to be even higher for turbulent flows ($\sim$50% of reduction) [17]. Also, it was shown that biofouling activity could be suppressed on SHPo surfaces due to the reduced areas of contact with water [21].

B. Wetting of SHPo Surface in Water

Despite the aforementioned desirable properties for underwater applications, no SHPo surface was shown to demonstrate the nonwetting properties while underwater in realistic conditions. The SHPo surfaces with structural pitch in micrometers [11], [14], [15] would stay nonwet only under low liquid pressure (e.g., < 2 kPa above ambient) for a limited time—valid only for laboratory tests. Those with structural pitch in nanometers [12], [13] may stay nonwet under reasonable liquid pressures (e.g., > 10 kPa above ambient) but still for a limited time (less than several hours). In water, the air layer held in between surface structures becomes unstable immediately by the liquid pressure or over time by gas diffusion, leading to the collapse of the air layer and the filling of the surrounding water in between the surface structures (i.e., wetting transition) [14], [22], [26]. While the wetting transition has been widely studied with droplets and puddles of liquids in air [27], it has rarely been studied underwater, i.e., while completely submerged in water, until recently. Although either thermodynamic energy minimum [28], [29] or force balance [30] can be applied to both the cases of in air and in water, the wetting transition in water is more complicated. For example, while the wetting transition in air was influenced primarily by the liquid pressure, the transition in water was highly influenced by the concentration of the dissolved gas in the surrounding liquid [25] and the dynamic condition (e.g., the liquid velocity) [24] as well as the liquid pressure [25], [26]. It is worth noting that hierarchical structures, which frequently exhibited extreme SHPo state against droplets in air, did not necessarily help prevent the wetting transition in water. For example, a lotus leaf, known for its hierarchical morphology, became immediately

Manuscript received July 26, 2011; revised December 26, 2011; accepted January 1, 2012. Date of publication February 15, 2012; date of current version May 28, 2012. This work was supported by the Nanoscale Interdisciplinary Research Team, National Science Foundation, under Grant 0103562. Subject Editor K. F. Bohringer.

C. Lee was with the Department of Mechanical and Aerospace Engineering, University of California, Los Angeles, CA 90095 USA. He is now with the Laboratoire de Physique de la Matière Condensée et Nanostructures, University of Lyon 1, 69622 Villeurbanne, France (e-mail: choongyeop.lee@univ-lyon1.fr).

C.-J. Kim is with the Department of Mechanical and Aerospace Engineering, University of California, Los Angeles, CA 90095 USA (e-mail: cjkim@ucla.edu).

Color versions of one or more of the figures in this paper are available online at http://ieeexplore.ieee.org.

Digital Object Identifier 10.1109/JMEMS.2012.2184081

wet at mere 20 cm under the surface of water and remained wet even after it was taken out of the water [23].

C. Importance of Liquid Pressure for Wetting

The systematic studies of the wetting transition in water have been recently conducted on several types of SHPo surfaces [25], [26]. Without exception, the liquid pressure was shown to be a critically important factor for the occurrence of the wetting transition. Theoretically, the collapse pressure at which the wetting transition occurs is inversely proportional to the pitch of surface structures [30] ($\Delta P \sim \gamma/L$, where ΔP is the differential pressure of the liquid over the gas, γ is the surface tension, and L is the structural pitch). In agreement with theoretical prediction, it was shown that the wetting transition occurred at the varying liquid pressure ranging from 5 to 30 kPa above the ambient depending on microstructures [26]. It needs to be noted that most underwater applications (e.g., vessels and submarines) involve a much higher liquid pressure (e.g., > 100 kPa above ambient) than what have normally been tested under the laboratory conditions, implying that it would be more challenging to preserve a stable air layer in real applications. Even though the wetting transition by the high liquid pressure can be prevented by reducing the pitch of the structures down to nanometer scale [12], [13], the defense will be only temporary; the gas will be lost to the surrounding liquid by diffusion eventually, leading to the wetting of surface structures. In this diffusional wetting, the liquid pressure still plays a critical role, because a higher liquid pressure generally leads to the faster decay of the air layer on SHPo surfaces [25]. Even though Salvinia leaves can hold a gas layer for a relatively long time (up to several weeks) [31], they normally reside in shallow water under a low liquid pressure (much less than 1 kPa above ambient), where the gas loss by diffusion was expected to be much slower than most underwater conditions.

D. Recovery of SHPo State in Water

To date, no SHPo surface has been reported to stay SHPo while underwater for an extended period (e.g., days) in practical conditions (e.g., a liquid pressure higher than 50 kPa above ambient). It is further suspected that such an ideal surface cannot even exist, because the loss of trapped gas to the surrounding liquid by diffusion is inevitable. Rather, practical approaches would be to actively replenish the gas as it is diffused out from the SHPo surface. The active approach would be more robust if also the surface can be dewetted, i.e., recover the SHPo state, even after it gets wet, and it would be practical if the implementation of the approach is not too costly and does not consume too much energy.

Methods to recover the SHPo state while underwater have been reported most recently through an active means. By designing surface structures that make the gas spread on (rather than bubble off) the surface and implementing electrodes on the bottom surface, Lee and Kim [32] replenished the lost gas with an electrolytically generated gas. Such surfaces recovered the SHPo state from a fully wetted condition or withstood high water pressure (as high as seven times the ambient pressure, i.e., 6 atm above ambient) indefinitely.

E. Consideration for Drag Reduction

Considered the most exciting underwater application of the SHPo surfaces has been reduction of skin friction. However, the drag reduction has never been proven in a realistic condition, because it requires that the surface maintains an SHPo state in the first place. For a structured hydrophobic surface to resist the wetting transition even for a short time, the surface structures need to be dense enough to withstand the liquid pressure. For a liquid pressure higher than 0.5 atm ($\sim$50 kPa or $\sim$5 m of water) above ambient—a pressure commonly found in many applications, surface structures of a submicrometer pitch are needed [12], [13]. Unfortunately, while the resistance against wetting is inversely proportional to the pitch [30]($\Delta P \sim \gamma/L, \Delta P$), the slip length is proportional to the pitch ($\delta \sim L$) [33]. As a result, the surface structures with a submicrometer pitch—necessary to stay SHPo against a pressure—would induce a slip length around 200 nm [13], which is not large enough to benefit regular-scale flow systems. This dilemma can be overcome if the surface structures are built in a hierarchical way and an active means of gas recovery is used, which is as follows. Consider hydrophobic microstructures (i.e., primary structures) constructed on a substrate covered with hydrophobic nanostructures (i.e., secondary structures). After the primary structures get wet under a liquid pressure, the secondary structures on the bottom surface can hold a gas layer against the pressure due to their small pitches and remain SHPo. The SHPo bottom surface will assist in dewetting of the primary structures during the subsequent recovery phase. Meanwhile, the slippage effect depends only on the microstructures, as long as they are nonwetted; the nanostructures do not affect the amount of slip over the microstrucrtures. Therefore, if a method of gas recovery is provisioned to an SHPo surface of hierarchical construction, the surface may possess both the resistance against liquid pressure and a large slippage effect.

F. Current Study

In this paper, we investigate the wetting and dewetting characteristics of hierarchical SHPo structures, built in the aforementioned way and proven capable of recovering the SHPo state while underwater [32]. Different ways to dewet a wetted surface are introduced, e.g., changing the environment outside the surface and generating gases inside structured surfaces. After presenting the fabrication of the hierarchically constructed surface structures integrated with patterned electrodes on the substrate and the rationales for the hierarchically constructed surface structures, wetting and dewetting of the surfaces are studied. We further show that our surface is functional even in two adverse conditions expected in engineering practices (i.e., high liquid pressure and defective surface).

II. Experimental Details

A. Sample Fabrication

To study dewetting, i.e., recovery of the SHPo state, while underwater, one has to supply a gas to the already wetted surfaces while underwater. Although such a supplied gas has a strong tendency to form bubbles and leave off the

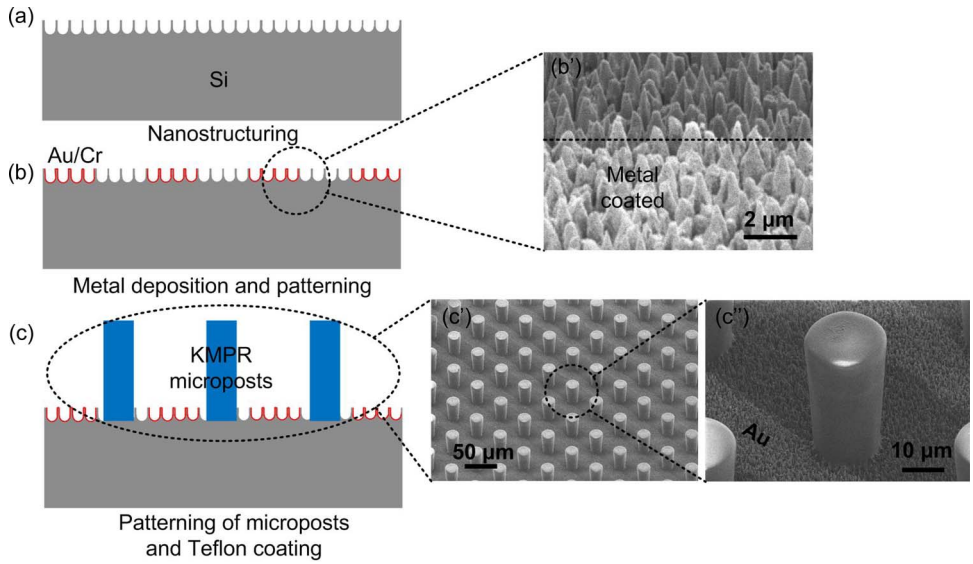

Fig. 1. Fabrication process of the hierarchical SHPo surfaces tested for underwater applications. (a) Nanoposts are formed on the silicon surface. (b) Au/Cr layer is deposited and patterned as electrodes for electrolysis. (b′) SEM image shows the patterned metal electrodes on nanoposts. (c) Microposts are built on the nanostructured substrate out of a negative photoresist (KMPR), and all the surfaces are coated with a thin layer of Teflon AF. (c′) SEM image of the completed hierarchical structures before Teflon coating. (c″) Magnified SEM image showing one micropost and the bottom surface.

microstructured surface, it can indeed form a stable gas layer if the microstructures satisfy certain geometric criteria [32]. For a square array of circular microposts, the geometric criteria can be expressed as the following [32]:

$$\frac{-\cos\theta_{b,\mathrm{rec}}}{\left[2\sin\theta_{p,\mathrm{rec}}\left(1-\sqrt{\pi(1-\phi)}/\phi\right)\right]} > H/L > \frac{\left(\sqrt{2}-2\sqrt{(1-\phi)/\pi}\right)(-1+\sin\theta_{p,\mathrm{adv}})}{2\cos\theta_{p,\mathrm{adv}}}. \quad (1)$$

Here, ϕ, H, L, and θ are the air fraction (i.e., $1-\pi D^2/4$, where D is the diameter of post), height and pitch (i.e., center-to-center distance between posts) of the posts, and contact angle (CA), respectively. For the CA θ, the subscripts adv and rec mean advancing and receding, respectively, and subscripts p and b mean on the surface of the posts and on the bottom surface between the posts, respectively. The aforementioned criteria are derived based on two conditions. The first condition is that the resistance against the spreading of gases in between microposts should be smaller than that against the growth of gases over the top surface of microposts (left inequality). The second condition is that there should be no premature destabilization of a gas film, i.e., the liquid–gas interface should not touch the bottom surface (right inequality).

Our target surface in this paper consists of a square array of hydrophobic microposts, whose geometry (i.e., pitch, height, and gas fraction) meets the aforementioned criteria, on a substrate covered with a random or square array of hydrophobic nanoposts. The overall fabrication process is shown in Fig. 1. First, in Fig. 1(a), we generated nanoposts on 4-in Si wafer using two different methods: black silicon method and interference lithography. The black silicon method formed sharp nanoposts of random distribution with a typical height ranging between 1 and 5 μm and a typical pitch ranging between 0.5 and 1 μm. The process followed a specifically tuned recipe [2] to etch a blank Si substrate in deep reactive ion etcher (DRIE) for 40 min. The interference lithography and a subsequent DRIE process [8] generated a square array of nanoposts with $\sim$250-nm height and 250-nm pitch. Due to its relative simplicity in fabrication, the black silicon method was used to fabricate most of the samples in the present study, while the interference lithography was used to prepare some of the samples tested for high liquid pressure, to be explained later.

After generating nanoposts on a silicon substrate, the electrodes for electrolysis were fabricated, as shown in Fig. 1(b), first by depositing 10-nm-thick Cr and 200-nm-thick Au layers successively on the substrate by electron-beam evaporator. Despite the high aspect ratio of the nanoposts, a positively tapered sidewall of nanoposts helped the coating as confirmed by the SEM image in Fig. 1(b′) and conductivity measurement. Then, 8-μm-thick AZ 4620 photoresist was spin coated and defined in the form of parallel lines by photolithography. The Cr/Au was then wet etched to form a set of metal lines of 20 μm in width and 50 μm in pitch. The metal layer was patterned, anticipating that both the anode and cathode for electrolysis may eventually be placed on the surface. The remaining photoresist was removed by acetone, methanol, deionized water rinsing, and O_2 plasma. Construction of microposts on the substrate full of Si nanoposts is shown in Fig. 1(c). A negative photoresist (KMPR 1050, Microchem) was spin coated and defined using photolithography. The photoresist became the final micropost structures of a fixed height (50 μm) and varying pitches (50 and 100 μm) and gas fractions (85%, 90%, 95%, and 98%), as shown in Fig. 1(c′) and (c″). To make all the surfaces hydrophobic, 2% Teflon AF (Dupont) solution was spin coated on the wafer (thickness expected on the order of 200 nm on the flat surface), followed by a thorough rinsing with perfluorocompound FC-40 (Acros Organics) to remove the excess Teflon, particularly on the nanostructures. The thickness of Teflon was estimated to be 20–40 nm, based on an atomic force microscopy study of identically processed Teflon on a flat

surface. Most of the tests in this study used a sample cleaved out of the aforementioned processed wafer to be 1.8 cm on a side.

B. Wetting Experiments

The wetting and dewetting experiments were conducted using tap water without purification. In the present study, two different approaches were used to induce the wetting transition, i.e., nonwetting-to-wetting or Cassie-to-Wenzel transition, on the SHPo surfaces prepared previously. The first approach was to subject the experimental setup to a moderate vacuum (1–2 kPa below ambient). Wetting was dependent on the resident time inside the vacuum environment, as expected. Once the vacuum (1–2 kPa below ambient) was applied, the microposts (used: 50- and 100-μm pitches and varying air fractions of 85%, 90%, 95%, and 98%) started to get wet immediately (and completed wetting the entire surface in 2–3 min), and the nanoposts (0.5–1-μm pitch and nominal air fraction over 95%) started to get wet soon ($\sim$3 min) after all the microposts were wetted (and completed wetting the entire surface in 3–4 min). Please note that the nanostructures started to be wetted only after the microposts were completely wetted. Once wetted, the surfaces did not recover the nonwetted state by removing the vacuum. In the present experiment, the resident time inside the vacuum environment was limited to less than 3 min to ensure that the microstructures were wetted but not the nanostructures. Similarly, it was possible to induce the wetting by placing the SHPo surface in water that had already been degassed, e.g., by vacuum over 3 min.

The second approach to wet the SHPo surfaces was to pressurize the surrounding liquid. The sample was placed inside a custom-made pressure chamber, which was filled with water and connected to a nitrogen tank. The liquid pressure was controlled in the range between 1 atm (i.e., ambient pressure) and 7 atm by regulating the pressure of the nitrogen gas above the water. The fact that one can wet the SHPo surface by either vacuuming or pressurizing indicates the frailness of the SHPo state in water.

C. Dewetting Experiments

Most of dewetting experiments, i.e., wetting-to-nonwetting or Wenzel-to-Cassie recovery, were conducted on a vibration isolation table under a 50–200$\times$ optical microscope connected to a video recorder. When electrolysis was used to generate the gas for dewetting, the Au electrodes on the nanostructured bottom surface and covered with a thin layer of Teflon were used as the cathode generating H_2 gases, while a copper wire placed $\sim$1 cm above the sample surface was used as the anode. The operating voltage for electrolysis was fixed at 10 V, most of which was to overcome the resistance across the thin Teflon and through the electrical arrangement between the sample and the instruments.

III. Results and Discussion

A. Wetting by Gas Diffusion

For all the experiments in this study, the samples were placed at the bottom of a laboratory beaker filled with a few centimeters of water. Under this small hydraulic pressure (much lower than 1 kPa above ambient), all the microposts on the SHPo surfaces remained nonwet. However, the microposts (tested: 50-μm pitch and 90% air fraction) started to get wet after several hours (and completely wetted in several days), as the trapped air was diffused out to the surrounding water, and the nanoposts at the bottom started to get wet after the microposts were completely wetted. It is worth noting that, if the water had been degassed before the test, the wetting started much sooner: several seconds for the microposts (completed in several minutes) and several minutes for the nanoposts.

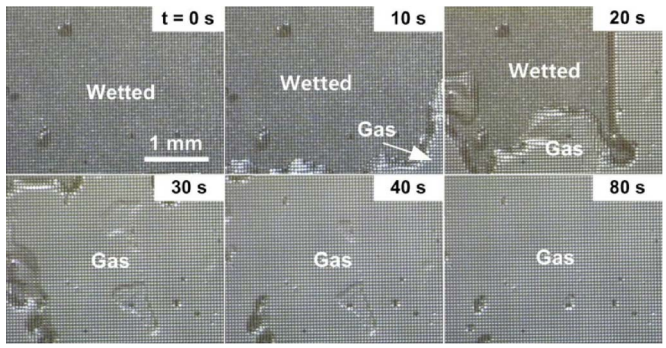

Fig. 2. Wetting and dewetting of the hierarchical surface (tested microposts: 50-μm pitch and 90% gas fraction) in water by gas diffusion. The sample had first been placed in degassed water, letting the air on the surface diffuse away and wetting all the microposts (entire surface) in 2 min. At 0 s, fresh (aerated) water was added to the beaker. With the air concentration of the water increased, dewetting has ensued, as shown, apparently because gas started to diffuse back into the surface structures.

After the surface (microposts) was wetted, we were able to recover the nonwetted state by adding fresh tap (aerated) water to the degassed water, as far as the addition was done before the nanoposts got wet, as shown in Fig. 2. The aforementioned experiments indicate that the wetting transition by gas diffusion is a direct manifestation of thermodynamic imbalance between the gas layer on the SHPo surfaces and the gas dissolved, usually not saturated, in the liquid. Numerous examples of wetting transition but almost no example of dewetting transition on SHPo surfaces in water support the natural tendency to lose the SHPo state and difficulty of recovering it. It may be possible to prevent the diffusional gas loss by controlling the gas concentration in the surrounding water, which is unfortunately impractical in most real applications.

B. Dewetting by Breathing

Dewetting can be achieved, if there is a passage between the surface microstructures and an air source, e.g., the air outside the liquid, as shown in Fig. 3. For the sample in Fig. 3 (microposts: 50-μm pitch and 90% air fraction), the surface above the water was smooth, and the structured surface started slightly below the water level. Note that the entire structured area was submerged in water before the test started. First, the SHPo surface was made wet by subjecting the experimental setup to a vacuum. However, as soon as a part of the structured area was exposed to the outside air while pulling the sample up, air was suddenly entrained onto the structured surface (i.e., the microposts were dewetted) and started to propagate downward.

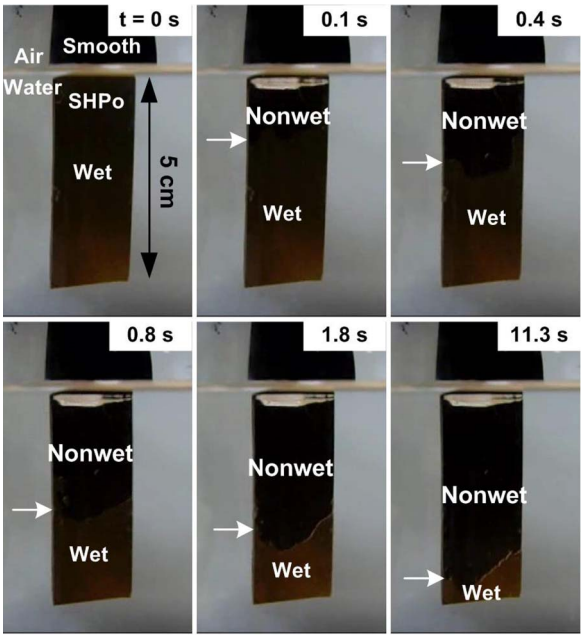

Fig. 3. Dewetting of the wetted hierarchical surface in water by entraining the outside air (tested microposts: 50-μm pitch and 90% gas fraction). The top part of the sample has a smooth surface, and the structured surface starts slightly below the water level. After making the surface structures wet by subjecting the setup to a moderate vacuum, the sample was slowly raised. As soon as the top end of the structured region (wetted) was exposed to the air above water (between 0 and 0.1 s), air was entrained into the surface structures, initiating the dewetting. A thick silvery line on the SHPo surface right below the water surface (after 0.1 s) indicates an air–water interface connecting the outside air to the surface structures. The white arrows indicate the location of the advancing air front on the sample surface. Note that the advancing is fast at beginning and slows down as the air front propagates deeper in the water.

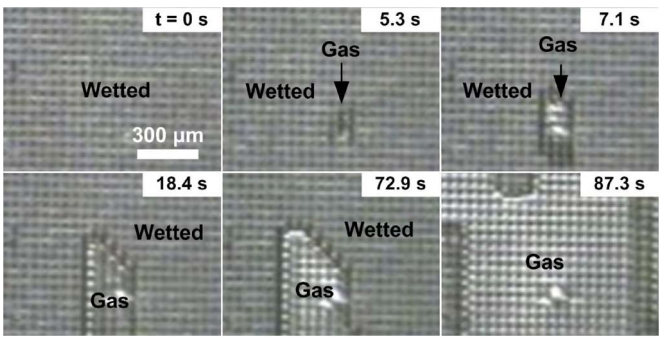

Fig. 4. Formation of a gas layer by electrolysis (microposts: 50-μm pitch and 85% gas fraction). Dewetting began with the nucleation of a gas (5.3 s), followed by the propagation of gas film into the surrounding area.

It needs to be noted that, when the structured surface was exposed to the air (0.1 s in Fig. 4), a curved air–water interface (connecting the air outside the water to the surface structures) appeared as a thick silvery line on the sample surface right below the water surface. It was instructive that the dewetting slowed down as the gas film advanced deeper into the water and the hydrostatic pressure increased. How deep would the dewetting propagate by this breathing approach depends on the geometry of the microstructures.

In our test, the dewetting did not propagate deeper than 5 cm, which is consistent with the liquid pressure calculated to induce a wetting transition on the microposts (50-μm height, 50-μm pitch, and 90% air fraction), i.e., $\sim$0.5 kPa above the ambient. In any case, the aforementioned test suggests that it is possible to design indefinite SHPo surfaces for shallow-water applications.

C. Gas Generation

Unless the water is saturated with air, a gas needs to be actively provided to the surface in order to prevent the wetting by gas diffusion or recover an already wetted surface. Generally, gases can be made available by thermal, chemical, electrochemical, and pneumatic methods, among which we deemed the electrochemical the most suitable for our goal. As described in the experimental section, we could easily pattern electrodes on the substrate of the microposts. Compared with pneumatic methods, which would require a pump, feeding lines, and a source of gas, for example, [34], generation of gases by electrolysis using the built-in electrodes and the surrounding water is much simpler. Compared with chemical methods, which would require specific combinations of materials that would be consumed, for example, [35], the electrolytic method would be more practical. While thermal methods generate vapors, which would not only consume significant energy [37] but also collapse as soon as the heat is removed, e.g., in a fraction of a second, the electrolysis generates gases, which would be dissolved into the water in hours [36]. Regarding the potential degradation of the metal electrodes for electrolysis under a corrosive environment (e.g., seawater), we note that electrodes will be protected from the corrosive environment by the gas layer most of the times. Moreover, electrolysis has been widely employed as a preferred gas generation method for drag reduction by microbubble injection [38]–[40] without any serious safety issues due to the generated gases.

D. Dewetting by Electrolysis

After the microposts on the surface (but not the nanoposts on the bottom) were wetted inside the vacuum, 10 V was applied across the two electrodes (the cathode on the bottom surface and the anode inside the liquid pool) to initiate the electrolysis.

The dewetting process began with gas nucleation at random locations on the sample surface (microposts: 50-μm pitch and 85% air fraction), one of which is shown over time in Fig. 4. The nucleated gas (at 5.3 s) started to expand to the surrounding areas as a film by absorbing the generated gases from them, until it merged to the neighboring patches of gas films. This mode of gas film formation (i.e., preferential growth of a single large gas bubble) is due to the fact that gases on the surface are connected to each other via a residual gas layer on nanostructures. When a gas bubble is connected to smaller gas bubbles through a residual gas layer, gases inside smaller bubbles are transported to a larger bubble due to the pressure difference, resulting in the continuous growth of a single large bubble.

The time sequential images in Figs. 5 and 6 show the gradual propagation of a gas film on all the hydrophobic hierarchical surfaces fabricated for this study, starting with a wetted state over the entire surfaces and completing when the entire surfaces

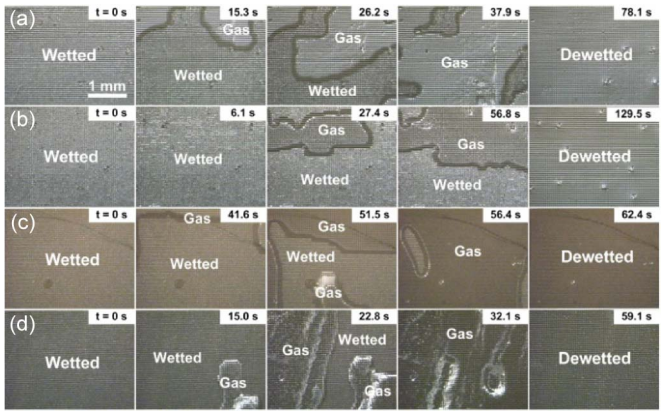

Fig. 5. Dewetting by electrolysis of microposts with a pitch of 50 μm and gas fractions of (a) 85%, (b) 90%, (c) 95%, and (d) 98%.

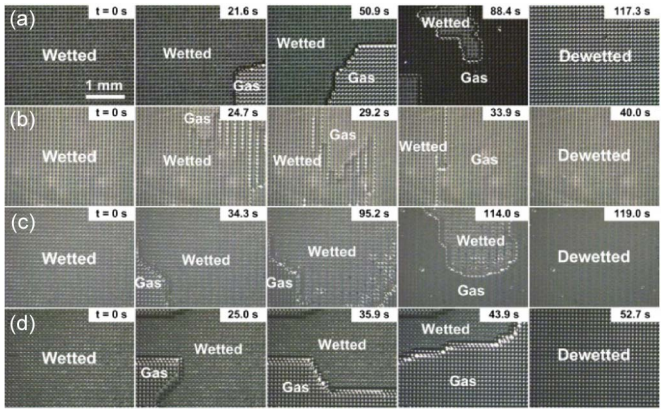

Fig. 6. Dewetting by electrolysis of microposts with a pitch of 100 μm and gas fractions of (a) 85%, (b) 90%, (c) 95%, and (d) 98%.

were dewetted. Fig. 5 shows the tests on the microposts with a fixed pitch of 50 μm and varying gas fractions of 85%, 90%, 95%, and 98%. Fig. 6 shows the tests on the microposts with a fixed pitch of 100 μm and the same varying gas fractions. In both cases, dewetting was generally completed within several minutes. The process variation in the black silicon method caused the different color of each sample and probably also contributed to the difference in the total time required for dewetting. As a result, no direct correlation between the total time needed for dewetting and the gas fraction (i.e., the space to fill with a gas) was observed in the present study. During dewetting, the fluctuation of the liquid–gas interface on the microposts resulted in the color and darkness variation in the reflection, as shown best in Fig. 6(a).

E. Role of the Nanostructured Bottom

The aforementioned dewetting tests in Figs. 4–6 started after the entire area of the samples was wetted; they were the worst case scenarios. It would take less time and energy to complete dewetting, if less area were wetted. During the wetting transition, usually, the wetting starts on small regions and propagates to the surrounding area.

It would help if we can minimize the propagation when some spots get wet perhaps accidentally. To test how wetting propagates on our hierarchically structured surface, we created

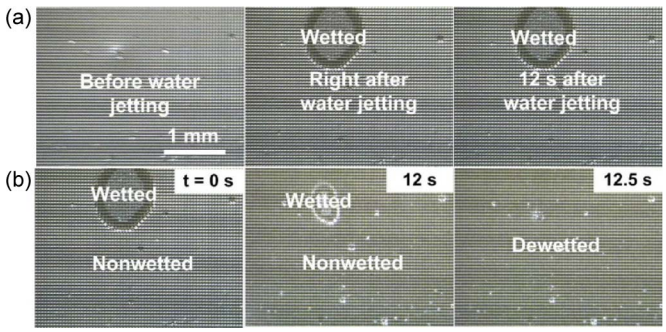

Fig. 7. Hierarchical surface resists against wetting propagation when locally wetted, rendering dewetting easier. (a) For the testing (microposts: 50-μm pitch and 95% gas fraction), the local wetting was induced by jetting water from a syringe in water. The wetted area remained unchanged over time, as the SHPo bottom surface confined the wetted area from spreading. (b) When the electrolysis was initiated ($t = 0$ s), the small wetted area was subsequently dewetted.

a local wetting, as shown in Fig. 7(a), by jetting water onto the surface in an SHPo state with a syringe while immersed in water. While the jetted spot became wet, the SHPo bottom surface resisted propagation of the wetting, and the wetted area did not increase over time. The same microposts on a smooth bottom would have seen the wetting propagate to the entire sample area. The confined wetted area easily recovered a nonwetted state by electrolysis within 20 s in Fig. 7(b), compared with the 60 s on the same geometry in Fig. 5(c). In addition to directing the gas to grow laterally between microposts for them to recover the nonwetted state (i.e., SHPo state) while underwater [32], the nonwetting nature of the nanostructured bottom (thus, SHPo on its own) prevented the wetting propagation across the microposts when wetting occurred locally.

F. Power Consumption

Electrolysis on the reported surface is self-controlled, i.e., the electrolysis occurs only when the gas layer needs additional gas without any external or feedback control.

If water wets any microposts and contacts the bottom surface under them, electrochemical circuits close, and a gas is generated at the contact by electrolysis; when the gas covers the electrode, the circuit becomes open, and the electrolysis stops. While this self-limiting, i.e., self-activating and self-terminating, electrolysis worked in principle, there was a leakage current through the substrate even after the surface restored the nonwetted state. The leakage current was significantly reduced by covering most of the substrate area outside the structured region with an adhesive tape to prevent the contact with the water, but the leakage was not completely eliminated in our current experiments. Although the electric current during the dewetting decreased (from 3 to less than 1 mA after the aforementioned passivation of the nonstructured region), the leakage was still nonnegligible (between $\sim$0.1 and 1 mA). This corresponds to 2–8-mW input power per 1 cm^2 for dewetting process and 0.2–2-mW additional power consumption per 1 cm^2 due to the leakage. While the leakage calls for an improvement of experimental setup and procedure to accurately assess the power needed for the electrolytic recovery, it suggests that the

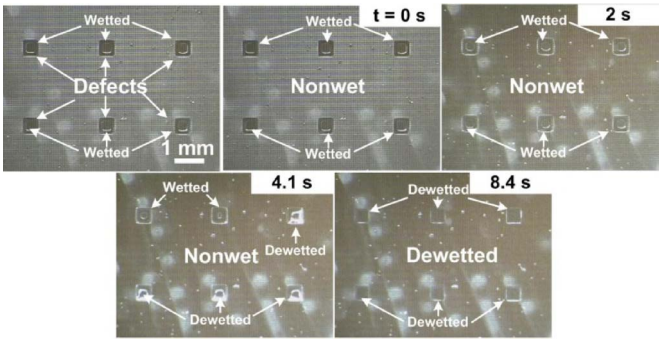

Fig. 8. Dewetting in the presence of defects (microposts: 50-μm pitch and 85% gas fraction). The wetted areas were confined to the defected areas due to the SHPo nature of the nanostructured bottom surface and did not spread to the surrounding area over time. The second image was taken 5 s after the first image, and there was no noticeable change in the wetted area. When the voltage was applied ($t = 0$ s), the wetted area was easily dewetted by electrolysis.

net power needed for the electrolytic dewetting is much smaller than the current measurement. Theoretically, i.e., based on Faraday's law of electrolysis, 40–50 mC (less than 1 mA when dewetting is completed in 1 min) is needed to recover 1 cm^2 of the current sample surfaces from a wetted to a nonwetted state, corresponding to $\sim$1-mW power consumption per 1 cm^2 when an activation voltage of 1.25 V is used for calculation.

G. Defective SHPo Surfaces

To explore the implications of the electrolysis-assisted underwater SHPo surfaces in practical applications, we further tested dewetting under two simulated unfavorable conditions: defective surface and high hydraulic pressure. First, we artificially created defected areas, each 0.5 mm by 0.5 mm, by removing microposts in the area, as shown in Fig. 8. As some of the many foreign objects in the water will collide onto the SHPo surface in applications and dense objects may cause damages, the SHPo recovery should reliably work in the presence of defects, or at least the wetting on the defects should not propagate to the undamaged areas.

While the surface inside the defective area of missing posts gets wet immediately under any liquid pressure, the wetting did not propagate to the adjacent nondefective area due to the SHPo bottom surface. The second image in Fig. 8, taken 5 s after the first image, shows no propagation of wetting. When electrolysis was initiated ($t = 0$ s), the defective region was covered with a gas layer, demonstrating the effectiveness of the electrolysis-based approach to overcome the surface defects. Of course, the defective areas will draw electric current continuously to remain covered with a gas.

H. Dewetting Under Pressure

The main disjoint between almost all the drag-reduction research of the SHPo surfaces and the implementation to applications has been the existence of large hydrostatic pressure in most realistic situations. Here, we elaborate how the electrolysis-based hierarchical surfaces, first presented by Lee and Kim [32], restore a gas layer under realistic liquid pressures. The approach was effective as long as the bottom surface

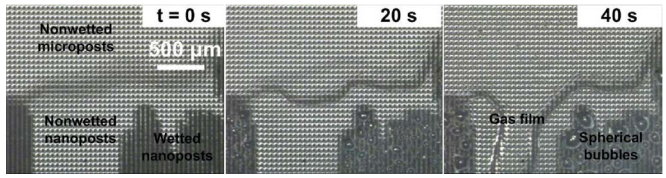

Fig. 9. Gas generation by electrolysis when some of the nanoposts are wetted (by an intentional liquid pressure of 700 kPa above ambient, i.e., 1.7 atm). While a gas film was formed on nonwetted nanoposts, spherical bubbles were formed on the wetted nanoposts.

remained SHPo, i.e., the nanostructures on the bottom were maintained nonwet. In most of the current report (i.e., liquid pressure at 0–1 kPa above ambient), the nanoposts remained nonwet after the microposts were wetted (the microposts began wetting at $\sim$0.5 kPa above ambient). However, the nanoposts could be wetted too by pressurizing the liquid to 1.5–2 atm (i.e., 500–1000 kPa above ambient). Once the nanoposts were wetted, increasing $\theta_{b,\mathrm{rec}}$ in (1) and tightening the recovery criteria, at activation of electrolysis, spherical gas bubbles were formed instead of the desired gas film, as shown in Fig. 9, failing to dewet the surface. We have performed the dewetting tests under the highest pressures that we could apply which wetted the microposts but not the nanoposts: between 1.4 and 1.7 atm. As the liquid pressure was increased, the wetting occurred on some locations and started to propagate. Note that only the microposts became wet during the experiment. When the power was turned on to start the electrolysis, the surface was dewetted in much the same way as shown in Figs. 5 and 6 over 2–4 min, slower because more gas has to be generated to fill the same volume under a higher pressure. In addition, we have tested the same microposts on the nanoposts made by the interference lithography, which have an exact pitch of 0.25 μm. Since these nanoposts were more stable due to their smaller pitches, we were able to apply higher pressures to wet the microposts without wetting the nanoposts: between 3 and 4 atm. We have obtained the same success with this sample in dewetting the wetted microposts although even slower (more than 5 min) due to the higher compression.

I. Staying SHPo Under a High Pressure

So far, we have considered rather pessimistic situations, i.e., recovering the nonwetting state after the microposts were already wetted, to be conservative in evaluating the developed SHPo surfaces. However, a more common scenario would be the surfaces maintaining an SHPo state most of the times and encountering problems (e.g., surface damage) occasionally on some spots. Under this condition of no intentional wetting, the microposts would recover the SHPo state by the electrolysis as soon as they get wet, and the nanoposts on the bottom would not encounter the danger of getting wet. This much-relaxed condition allowed us to test much higher liquid pressures, as shown in Fig. 10. Note that, even if there was no loss of mass, the gas on the SHPo surface was compressed when the liquid pressure increased. The resulting reduction of gas volume was continuously replenished by the electrolystically generated new gas. Since the gas generation continued until

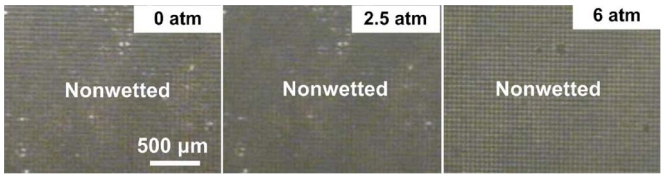

Fig. 10. Developed SHPo surface remained nonwet in water of an increasingly high pressure, when the voltage was kept on—tested up to 7 atm.

the gas pressure balanced with the increasing liquid pressure, the surface remained SHPo under liquid pressures much higher than all the tests so far. Fig. 10 shows the surface remaining nonwet at very high liquid pressures (up to 7 atm, only limited by the maximum pressure of the nitrogen gas used). Note that the nanoposts (made by the black silicon method) could not have withstood such high liquid pressures if the microposts were wetted. Incidentally, we could not observe the wetting and recovery cycles, perhaps because the cycles were too fast to visualize or electrolysis occurred through the moisture inside the gas layer, calling for future studies. As expected, this approach was effective only when the gas generation could catch up with the volume loss by the increasing pressure (0.5 atm/min in the present case). When the pressure was increased too fast (e.g., more than 1 atm/min), the wetting ensued on the surface.

IV. Conclusion

We have investigated the wetting and dewetting processes of the hydrophobic hierarchical surface structures (microposts on nanoposts) fabricated to meet the recently reported criteria for a gas recovery while underwater. While the wetting occurs naturally, the dewetting was obtained by active means. In the given configuration of surface structures, the nanoposts on the bottom confer the high CA and resistance against the wetting under the liquid pressure—the two properties required to dewet the wetted microposts—while the microposts provide a large slippage effect, which is crucial for drag-reduction application. On the tested surfaces, dewetting could be achieved by various active means, such as increasing air concentration in the water, bridging the structured surface to the air outside the water, and generating gases from the bottom surface using electrolysis. In particular, with electrolysis, it was possible to maintain the SHPo state in near-real environment such as defected surfaces and high liquid pressure. Still, there are several issues to be addressed for practical SHPo surfaces. First, with electrolysis, the SHPo surface was found degrading after several hours of operation, such as the Teflon on nanostructures getting delaminated. Also, there still remain the practical issues such as the manufacturability of the presented surface on a large scale and the effective placement of both electrodes on the surface. We have presented our findings to help ameliorate the design of SHPo surfaces for underwater applications and bring the potentials of SHPo surfaces to reality. Our results suggest that it is feasible to design structured surfaces that can retain the SHPo state for a long time even under the challenging underwater conditions.

Acknowledgment

The authors would like to thank Prof. C.-H. Choi for the help with nanostructured samples by interference lithography and H. Park for the help with the atomic force microscopy measurement of the Teflon thickness.

References

[1] W. Barthlott and C. Neinhuis, "Purity of the sacred lotus, or escape from contamination in biological surfaces," *Planta*, vol. 202, no. 1, pp. 1–8, Apr. 1997.
[2] J. Kim and C.-J. Kim, "Nanostructured surfaces for dramatic reduction of flow resistance in droplet-based microfluidics," in *Proc. 15th IEEE Int. Conf. MEMS*, Las Vegas, NV, 2002, pp. 479–482.
[3] R. Blossey, "Self-cleaning surfaces—Virtual realities," *Nat. Mater.*, vol. 2, no. 5, pp. 301–306, May 2003.
[4] X. Feng and L. Jiang, "Design and creation of superwetting/antiwetting surfaces," *Adv. Mater.*, vol. 18, no. 23, pp. 3063–3078, Nov. 2006.
[5] X.-M. Li, D. Reinhoudt, and M. Crego-Calama, "What do we need for a superhydrophobic surface? A review on the recent progress in the preparation of superhydrophobic surfaces," *Chem. Soc. Rev.*, vol. 36, no. 8, pp. 1350–1368, Aug. 2007.
[6] C. Dorrer and J. Ruhe, "Some thoughts on superhydrophobic wetting," *Soft Matter*, vol. 5, no. 1, pp. 51–61, Jan. 2009.
[7] D. Quere, "Wetting and roughness," *Annu. Rev. Mater. Res.*, vol. 38, pp. 71–99, Aug. 2008.
[8] C.-H. Choi and C.-J. Kim, "Fabrication of a dense array of tall nanostructures over a large sample area with sidewall profile and tip sharpness control," *Nanotechnology*, vol. 17, no. 21, pp. 5326–5333, Nov. 2006.
[9] A. Nakajima, A. Fujishima, K. Hashimoto, and T. Watanabe, "Preparation of transparent superhydrophobic boehmite and silica films by sublimation of aluminum acetylacetonate," *Adv. Mater.*, vol. 11, no. 16, pp. 1365–1368, Nov. 1999.
[10] Y. Xiu, Y. Liu, D. W. Hess, and C. P. Wong, "Mechanically robust superhydrophobicity on hierarchically structured Si surfaces," *Nanotechnology*, vol. 21, no. 15, p. 155 705, Apr. 2010.
[11] J. Ou, B. Perot, and J. P. Rothstein, "Laminar drag reduction in microchannels using ultrahydrophobic surfaces," *Phys. Fluids*, vol. 16, no. 12, pp. 4635–4643, Nov. 2004.
[12] C.-H. Choi and C.-J. Kim, "Large slip of aqueous liquid flow over a nanoengineered superhydrophobic surface," *Phys. Rev. Lett.*, vol. 96, no. 6, p. 66 001, Feb. 2006.
[13] C.-H. Choi, U. Ulmanella, J. Kim, C.-M. Ho, and C.-J. Kim, "Effective slip and friction reduction in nanograted superhydrophobic microchannels," *Phys. Fluids*, vol. 18, no. 8, p. 087105, Aug. 2006.
[14] C. Lee, C.-H. Choi, and C.-J. Kim, "Structured surfaces for a giant liquid slip," *Phys. Rev. Lett.*, vol. 101, no. 6, p. 064501, Aug. 2008.
[15] C. Lee and C.-J. Kim, "Maximizing the giant liquid slip on superhydrophobic microstructures by nanostructuring their sidewalls," *Langmuir*, vol. 25, no. 21, pp. 12 812–12 818, Nov. 2009.
[16] C. Lee and C.-J. Kim, "Influence of surface hierarchy of superhydrophobic surfaces on liquid slip," *Langmuir*, vol. 27, no. 7, pp. 4243–4248, Apr. 2011.
[17] R. J. Daniello, N. E. Waterhouse, and J. P. Rothstein, "Drag reduction in turbulent flows over superhydrophobic surfaces," *Phys. Fluids*, vol. 21, no. 8, p. 085103, Aug. 2009.
[18] J. P. Rothstein, "Slip on superhydrophobic surfaces," *Annu. Rev. Fluid Mech.*, vol. 42, pp. 89–109, 2010.
[19] D. M. Huang, C. Cottin-Bizonne, C. Ybert, and L. Bocquet, "Massive amplification of surface-induced transport at superhydrophobic surfaces," *Phys. Rev. Lett.*, vol. 101, no. 6, p. 064503, Aug. 2008.
[20] J. Genzer and K. Efimenko, "Recent developments in superhydrophobic surfaces and their relevance to marine fouling: A review," *Biofouling*, vol. 22, no. 5, pp. 339–360, Jan. 2006.
[21] A. J. Scardino, H. Zhang, D. J. Cookson, R. N. Lamb, and R. de Nys, "The role of nano-roughness in antifouling," *Biofouling*, vol. 25, no. 8, pp. 757–767, Aug. 2009.
[22] R. N. Govardhan, G. S. Srinivas, A. Asthana, and M. S. Bobji, "Time dependence of effective slip on textured hydrophobic surfaces," *Phys. Fluids*, vol. 21, no. 5, p. 052001, May 2009.
[23] S. Herminghaus, "Roughness-induced non-wetting," *Europhys. Lett.*, vol. 52, no. 2, pp. 165–170, Oct. 2000.

[24] M. Sakai, A. Nakajima, and A. Fujishima, "Removing an air layer from a superhydrophobic surface in flowing water," *Chem. Lett.*, vol. 39, no. 5, pp. 482–484, Apr. 2010.
[25] R. Poetes, K. Holtzmann, K. Franze, and U. Steiner, "Metastable underwater superhydrophobicity," *Phys. Rev. Lett.*, vol. 105, no. 16, p. 166 104, Oct. 2010.
[26] P. Forsberg, F. Nikolajeff, and M. Karlsson, "Cassie–Wenzel and Wenzel–Cassie transitions on immersed superhydrophobic surfaces under hydrostatic pressure," *Soft Matter*, vol. 7, no. 1, pp. 104–109, 2011.
[27] E. Bormashenko, "Wetting transitions on biomimetic surfaces," *Philos. Trans. Roy. Soc. London A, Math. Phys. Sci.*, vol. 368, no. 1929, pp. 4695–4711, Oct. 2010.
[28] N. A. Patankar, "Transition between superhydrophobic states on rough surfaces," *Langmuir*, vol. 20, no. 17, pp. 7097–7102, Aug. 2004.
[29] A. Marmur, "Underwater superhydrophobicity: Theoretical feasibility," *Langmuir*, vol. 22, no. 4, pp. 1400–1402, Feb. 2006.
[30] C. W. Extrand, "Criteria for ultralyophobic surfaces," *Langmuir*, vol. 20, no. 12, pp. 5013–5018, Jun. 2004.
[31] W. Barthlott, T. Schimmel, S. Wiersch, K. Koch, M. Brede, M. Barczewski, S. Walheim, A. Weis, A. Kaltenmaier, A. Leder, and H. F. Bonn, "The Salvinia paradox: Superhydrophobic surfaces with hydrophilic pins for air retention under water," *Adv. Mater*, vol. 22, no. 21, pp. 2325–2328, Jun. 2010.
[32] C. Lee and C.-J. Kim, "Underwater restoration and retention of gases on superhydrophobic surfaces for drag reduction," *Phys. Rev. Lett.*, vol. 106, no. 1, p. 014502, Jan. 2011.
[33] C. Ybert, C. Barentin, C. Cottin-Bizonne, P. Joseph, and L. Bocquet, "Achieving large slip with superhydrophobic surfaces: Scaling laws for generic geometries," *Phys. Fluids*, vol. 19, no. 12, p. 123 601, Dec. 2007.
[34] C. F. Carlborg and W. van der Wijngaart, "Sustained superhydrophobic friction reduction at high liquid pressures and large flows," *Langmuir*, vol. 27, no. 1, pp. 487–493, Jan. 2011.
[35] R. F. Ismagilov, A. Schwartz, N. Bowden, and G. M. Whitesides, "Autonomous movement and self-assembly," *Angew. Chem.*, vol. 114, no. 4, pp. 674–676, Feb. 2002.
[36] C. Neagu, H. Jansen, H. Gardeniers, and M. Elwenspoek, "The electrolysis of water: An actuation principle for MEMS with a big opportunity," *Mechatronics*, vol. 10, no. 4/5, pp. 571–581, Jun. 2000.
[37] D. D. Meng, Y. Ju, and C.-J. Kim, "A comparative study of electrolysis and boiling for bubble-driven microactuations," in *Proc. 13th Int. Conf. Solid-State Sens., Actuators, Microsyst.*, Seoul, Korea, 2005, pp. 1263–1266.
[38] M. E. McCormick and R. Bhattacharyya, "Drag reduction of a submersible hull by electrolysis," *Nav. Eng. J.*, vol. 85, no. 2, pp. 11–16, Apr. 1973.
[39] B. R. Elbing, E. S. Winkel, K. A. Lay, S. L. Ceccio, D. R. Dowling, and M. Perlin, "Bubble-induced skin-friction drag reduction and the abrupt transition to air-layer drag reduction," *J. Fluid Mech.*, vol. 612, pp. 201–236, Oct. 2008.
[40] S. L. Ceccio, "Frictional drag reduction of external flows with bubble and gas injection," *Annu. Rev. Fluid Mech.*, vol. 42, pp. 183–203, 2011.

Choongyeop Lee received the B.S. degree and the M.S. degree in mechanical engineering from Seoul National University, Seoul, Korea, and the Ph.D. degree in mechanical engineering from the University of California, Los Angeles (UCLA), in 2010.

After one-year postdoctoral experience in the Microfluidics Group (Microfluidics, MEMS, and Nanostructures Laboratory), École Supérieure de Physique et de Chimie Industrielles, Paris, France, he became a Postdoctoral Fellow in the Laboratoire de Physique de la Matire Condensée et Nanostructures, University of Lyon 1, Villeurbanne, France. His research interests include fabrication of micro-/nanostructures and study of liquid transport over superhydrophobic surfaces and in nanofluidics.

Dr. Lee was a recipient of a Graduate Student Fellowship from the California NanoSystems Institute, UCLA, in 2005.

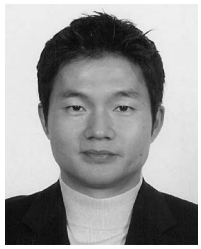

Chang-Jin "CJ" Kim (S'89–M'91) received the B.S. degree in mechanical engineering from Seoul National University, Seoul, Korea, the M.S. degree in mechanical engineering from Iowa State University, Ames, and the Ph.D. degree in mechanical engineering from the University of California, Berkeley, in 1991.

Since joining the faculty of the University of California, Los Angeles (UCLA), in 1993, he has developed several MEMS courses and established a MEMS Ph.D. major field in the Department of Mechanical and Aerospace Engineering in 1997. Directing the Micro and Nano Manufacturing Laboratory, he is also a founding member of the California NanoSystems Institute, UCLA. He has also been active in the commercial sector as a Board Member, a Scientific Advisor, a Consultant, and the Founder of start-up companies. He is currently serving on the Editorial Advisory Board for the *IEEJ Transactions on Electrical and Electronic Engineering*. His research interests are in MEMS and nanotechnology, including design and fabrication of micro/nano structures, actuators, and systems, with a focus on the use of surface tension.

Dr. Kim has served on numerous technical committees and panels, including Transducers, the IEEE International Conference on MEMS, and the National Academies Panel on Benchmarking the Research Competitiveness of the U.S. in Mechanical Engineering. He is currently serving on the Editorial Board of the JOURNAL OF MICROELECTROMECHANICAL SYSTEMS. As an ASME Fellow, he was the recipient of the Graduate Research Excellence Award from Iowa State University, the 1995 TRW Outstanding Young Teacher Award, a 1997 National Science Foundation CAREER Award, the 2002 Association for Laboratory Automation Achievement Award, and the 2008 Samueli Outstanding Teaching Award.